Reconstructing free-energy landscapes for cyclic molecular motors using full multidimensional or partial one-dimensional dynamic information

N. J. López-Alamilla and M. W. Jack[*]

Department of Physics, University of Otago, P. O. Box 56, Dunedin 9054, New Zealand

K. J. Challis

Scion, Private Bag 3020, Rotorua 3046, New Zealand

Diffusion on a free-energy landscape is a fundamental framework for describing molecular motors. In the landscape framework, energy conversion between different forms of energy, e.g., chemical and mechanical, is explicitly described using multidimensional nonseparable potential landscapes. We present a k-space method for reconstructing multidimensional free-energy landscapes from stochastic single-molecule trajectories. For a variety of two-dimensional model potential landscapes, we demonstrate the robustness of the method by reconstructing the landscapes using full dynamic information, i.e., simulated two-dimensional stochastic trajectories. We then consider the case where the stochastic trajectory is known only along one dimension. With this partial dynamic information, the reconstruction of the full two-dimensional landscape is severely limited in the majority of cases. However, we reconstruct effective one-dimensional landscapes for the two-dimensional model potentials. We discuss the interpretation of the one-dimensional landscapes and identify signatures of energy conversion. Finally, we consider the implications of these results for biological molecular motors experiments.

I. INTRODUCTION

Diffusion on a free-energy landscape is a fundamental framework for describing protein folding [1–10] and biological molecular motors [11–15]. Physical properties of molecular motors, such as drift velocity, diffusion coefficients [16–22], efficiency [15], force or torque generation [23,24], step sizes, and dwell times [25,26], can be derived from the free-energy landscape. Free-energy landscapes of particular molecular motors have been determined from molecular structure [4,27–30] or alternatively, in principle, could be reconstructed from increasingly available experimental single-molecule trajectories [2,3,6,7]. Reconstruction methods have so far only been developed for one-dimensional systems [31–35] and, therefore, do not in general apply to molecular motors that convert energy between two or more degrees of freedom. In this paper, we present a method for reconstructing multidimensional free-energy landscapes for cyclic molecular motors and show that it is robust in two dimensions when the full two-dimensional stochastic trajectories are known. We also consider what can be inferred about the two-dimensional landscape when the trajectory is known in only one dimension.

Free-energy landscape reconstruction methods are based on the Smoluchowski equation that describes overdamped Brownian motion on a time-independent free-energy potential landscape. First, the probability density for the system is determined from single-molecule trajectories and, then, the Smoluchowski equation is inverted to determine the landscape. The inversion step typically relies on a closed solution of the Smoluchowski equation that exists only in one dimension [21,31,32]. However, we recently developed a k-space method [34,35] that exploits the cyclic behavior of molecular motors and can be used for both equilibrium and nonequilibrium cases [34,35]. For one-dimensional systems, the k-space reconstruction method converges for increasing trajectory duration and sampling frequency [35].

Molecular motors convert energy from one form to another [16]. For example, the enzyme ATP synthase is composed of two molecular motors: The F_0 part uses a proton concentration gradient to drive rotation and the F_1 part uses the rotation to synthesize ATP. Within the energy landscape description, energy conversion between different forms of energy is explicitly described via a nonseparable potential landscape with at least two degrees of freedom [36–38].

The aim of this paper is to determine how landscape reconstruction methods based on single-trajectory analysis could be used to better understand energy conversion in molecular motors. In the first part of this work, we extend our k-space reconstruction method [34,35] to multiple dimensions. We use two-dimensional examples to show that a full reconstruction of the landscape is possible when the stochastic single-molecule trajectory is known in all relevant degrees of freedom. We contrast the accuracy and numerical expense of the full two-dimensional reconstruction with the one-dimensional case. In the second part of this work, we consider the case where the stochastic single-molecule trajectory is only known in one degree of freedom. This is common, for example, in mechanochemical molecular motors, where

_____
[*]michael.jack@otago.ac.nz

current experiments typically only measure the mechanical degree of freedom [18,39,40]. We explore to what extent, and under what circumstances, landscape reconstruction in only one degree of freedom can infer details of the full two-dimensional landscape and elucidate energy coupling.

The manuscript is ordered as follows. In Sec. II we review the Smoluchowski equation formalism used to model molecular motors and extend the one-dimensional k-space reconstruction method to multiple dimensions. In Sec. III we reconstruct two-dimensional landscapes for a variety of model potentials using simulated two-dimensional single-trajectories and demonstrate the accuracy and robustness of the method. In Sec. IV we consider the case where single trajectories are known only along one dimension. We show that it is always possible to reconstruct an effective one-dimensional potential along the measured degree of freedom but that it is often difficult to relate the one-dimensional potential to the full two-dimensional potential landscape. Despite this, we discuss the interpretation of the effective one-dimensional landscape and identify signatures of energy conversion. Section V concludes the paper.

II. MULTIDIMENSIONAL FREE-ENERGY LANDSCAPE RECONSTRUCTION

A. Landscape framework for molecular motors

Molecular motor dynamics are described as overdamped Brownian motion on a time-independent free-energy potential landscape and can be modelled via the multidimensional Smoluchowski equation [41]:

$$\frac{dP(\boldsymbol{r}, t)}{dt} = -\boldsymbol{\nabla} \cdot \boldsymbol{J}(\boldsymbol{r}, t), \tag{1}$$

where $P(\boldsymbol{r}, t)$ is the probability density for finding the motor at position $\boldsymbol{r}$ and time t and the probability current is

$$\boldsymbol{J}(\boldsymbol{r}, t) = -\frac{\Theta}{\gamma} \boldsymbol{\nabla} P(\boldsymbol{r}, t) - \frac{1}{\gamma} P(\boldsymbol{r}, t) \boldsymbol{\nabla} V(\boldsymbol{r}) \tag{2}$$

with γ the viscous friction coefficient, $\Theta = k_B T$, k_B the Boltzmann constant, and T the temperature. For the case of cyclic molecular motors, the potential landscape $V(\boldsymbol{r})$ is of the form $V(\boldsymbol{r}) = V_0(\boldsymbol{r}) - \boldsymbol{F} \cdot \boldsymbol{r}$, where $V_0(\boldsymbol{r}) = V_0(\boldsymbol{r} + L_j \hat{\boldsymbol{r}}_j)$ is a periodic potential with period L_j in the jth degree of freedom. The external force $\boldsymbol{F}$ drives the system out of equilibrium. The system dynamics can be described equivalently by the overdamped stochastic Langevin equation:

$$\dot{\boldsymbol{r}}(t) = -\frac{1}{\gamma} \boldsymbol{\nabla} V(\boldsymbol{r}) + \boldsymbol{\xi}(t), \tag{3}$$

where $\boldsymbol{\xi}(t)$ is a random Gaussian noise with zero mean and correlation $\langle \xi_j(t) \xi_{j'}(t') \rangle = 2\Theta \delta_{j,j'}(t - t')/\gamma$ [41]. This formulation is useful for simulating stochastic single-molecule trajectories analogous to the traces measured in experiments (see, for example, Ref. [8]).

To describe energy conversion in a molecular motor, the multidimensional free-energy potential landscape must be nonseparable [36]. Formally, the landscape can be written

$$V(\boldsymbol{r}) = \sum_j \mathcal{V}_j(r_j) + \mathcal{W}(\boldsymbol{r}), \tag{4}$$

where the separable term $\mathcal{V}_j(r_j)$ drives dynamics in the jth degree of freedom and the remaining nonseparable terms $\mathcal{W}(\boldsymbol{r})$ couple different degrees of freedom. Due to the non-separable terms of the potential, the steady-state distribution is not factorizable $P(\boldsymbol{r}) \neq \prod_j \mathcal{P}_j(r_j)$. The coupling means that the steady-state drift

$$\langle v_j \rangle = -\frac{1}{\gamma} \int d\boldsymbol{r} \, P(\boldsymbol{r}) \frac{\partial V(\boldsymbol{r})}{\partial r_j}, \tag{5}$$

is dependent not only on the force F_j but also on other components of the force, $F_{j'}$ where $j' \neq j$. The rate of change of work in each degree of freedom is [42]

$$\dot{W}_j = \frac{1}{\gamma} F_j \langle v_j \rangle. \tag{6}$$

If the drift v_j has the same sign as the force F_j in that degree of freedom, then the rate of change of work is positive. However, if the drift v_j and the force F_j have opposite sign, then the rate of change of work is negative. In this case work is being done against the external force and energy is being converted from one degree of freedom to another. Energy conversion increases when the system is tightly coupled, i.e., when the nonseparable coupling term $\mathcal{W}(\boldsymbol{r})$ dominates the potential $V(\boldsymbol{r})$, leading to the motion being confined to a coupled path through the landscape. In this case high-efficiency energy conversion can occur [36–38].

B. Multidimensional k-space landscape reconstruction

The k-space free-energy landscape reconstruction method developed in Refs. [34,35] can be generalized to multiple dimensions as follows. The periodicity of the potential means that both the steady-state probability $P(\boldsymbol{r})$ and steady-state current $\boldsymbol{J}(\boldsymbol{r})$ are periodic. Therefore, we expand them in their Fourier series as

$$V(\boldsymbol{r}) = -\boldsymbol{F} \cdot \boldsymbol{r} + \sum_{\boldsymbol{q}} V_{\boldsymbol{q}}^{\boldsymbol{0}} e^{i2\pi \boldsymbol{q} \cdot (\boldsymbol{r} \backslash \boldsymbol{L})}, \tag{7}$$

$$P(\boldsymbol{r}) = \sum_{\boldsymbol{k}} P_{\boldsymbol{k}} e^{i2\pi \boldsymbol{k} \cdot (\boldsymbol{r} \backslash \boldsymbol{L})}, \tag{8}$$

$$J_j(\boldsymbol{r}) = \sum_{\boldsymbol{k}} J_{j\boldsymbol{k}} e^{i2\pi \boldsymbol{k} \cdot (\boldsymbol{r} \backslash \boldsymbol{L})}, \tag{9}$$

where $\boldsymbol{F}, \boldsymbol{L}, \boldsymbol{k}, \boldsymbol{q}$ are vectors and $\boldsymbol{r} \backslash \boldsymbol{L}$ denotes a matrix with elementwise division such that $(\boldsymbol{r} \backslash \boldsymbol{L})_j = r_j / L_j$. The spectral component indices k_j and q_j take integer values bound by a finite maximum value $\mathcal{K}$, i.e., $k_j = 0, \pm 1, \pm 2, \dots, \pm \mathcal{K}$, and similarly for q_j.

Using Eqs. (7)–(9) we formulate the multidimensional steady-state Smoluchowski equation in k space as

$$\sum_{\boldsymbol{q} \neq \boldsymbol{0}} (\boldsymbol{q} \cdot \boldsymbol{k}) P_{\boldsymbol{k}-\boldsymbol{q}} V_{\boldsymbol{q}}^{\boldsymbol{0}} = -\left[(\Theta \boldsymbol{k}) \cdot \boldsymbol{k} - i\boldsymbol{k} \cdot \left(\frac{\boldsymbol{F} \circ \boldsymbol{L}}{2\pi} \right) \right] P_{\boldsymbol{k}},$$

$$\boldsymbol{k} \neq \boldsymbol{0}, \tag{10}$$

where $\boldsymbol{F} \circ \boldsymbol{L}$ denotes a matrix with elementwise multiplication such that $(\boldsymbol{F} \circ \boldsymbol{L})_j = F_j L_j$. Note that $P_{\boldsymbol{0}} = 1/\|\boldsymbol{L}\|$ is the normalization condition in k space with $\|\boldsymbol{L}\| = \prod_j L_j$ and $V_{\boldsymbol{0}}^{\boldsymbol{0}}$

is the reference level of the potential that has no physical implications. The k-space probability current components are given by

$$\gamma J_{j_k} = F_j P_k - i\frac{2\pi}{L_j}\left\{\sum_q q_j P_{k-q} V_q^0 + \Theta k_j P_k\right\}. \quad (11)$$

The drift velocity components are related to the k-space probability current by $\langle v_j \rangle = J_{j\,0} L_j$. For $k = 0$, Eq. (11) simplifies to

$$\gamma \langle v_j \rangle = \frac{F_j L_j}{\|\boldsymbol{L}\|} - i2\pi \sum_q q_j P_{-q} V_q^0, \quad (12)$$

which is the k-space representation of Eq. (5). Equation (12) provides the general relationship between the drift $\langle v_j \rangle$ and the force F_j and the dependence on other forces $F_{j'}$ is via P_k that depends on both $V_0(\boldsymbol{r})$ and $\boldsymbol{F}$.

To reconstruct the free-energy landscape, the steady-state probability density $P(\boldsymbol{r})$ is determined from stochastic single trajectories using a position histogram [34,35]. Equation (10) is then cast into matrix form and standard matrix inversion methods are used to calculate the Fourier coefficients of the free-energy landscape from the probability density. The reconstructed potential $V^R(\boldsymbol{r})$ in position space is then computed using the Fourier series Eq. (7).

When the value of the force $\boldsymbol{F}$ is known, the direct reconstruction of the free-energy landscape is straightforward as described above using Eq. (10) [34]. However, if one or more of the force components are unknown, the method can still be used via Eq. (12) and the drift velocity determined from the stochastic trajectories [18,39]. Equations (10) and (12) cannot be solved together because they lead to a singularity. Therefore, we use an iterative method to find a self-consistent solution of Eqs. (10)–(12). This involves making a guess for $\boldsymbol{F}$, calculating the landscape, recalculating $\boldsymbol{F}$, and so on. The iteration process stops once all unknown force components meet the tolerance condition

$$|F_{i,j} - F'_{i,j}| \leqslant \epsilon_j \quad \forall j, \quad (13)$$

where i is the iteration number and $\epsilon_j > 0$ is a small number representing the desired accuracy of the force component in the jth coordinate.

III. NUMERIC EXAMPLES OF TWO-DIMENSIONAL LANDSCAPE RECONSTRUCTION

In this section we illustrate the multidimensional k-space reconstruction method using a variety of model potentials. Although there may be many dimensions in general, we consider only two-dimensional potentials for the rest of the manuscript. This provides the simplest explicit treatment of energy coupling in a molecular motor. We consider four two-dimensional model potentials defined as follows. The first potential we consider is a simple potential constructed from cosines:

$$V_{CC}(x, y) = A_x \cos\left(\frac{2\pi x}{L_x}\right) + A_y \cos\left(\frac{2\pi y}{L_y}\right)$$
$$+ A_{xy} \cos\left(2\pi\left[\frac{x}{L_x} - \frac{y}{L_y}\right]\right) - F_x x - F_y y. \quad (14)$$
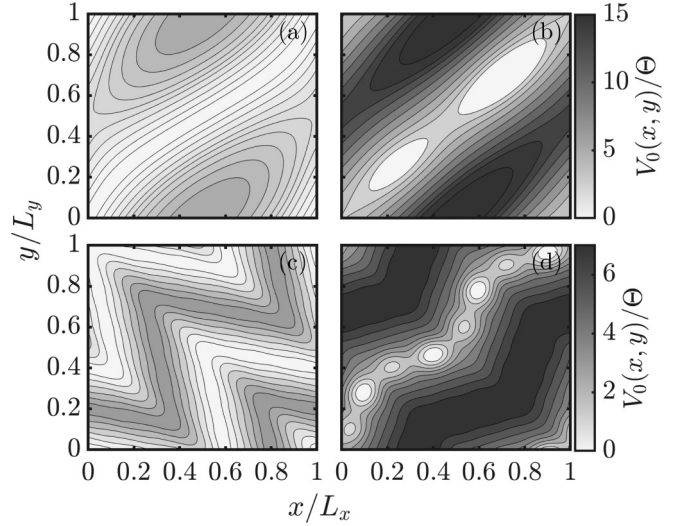
FIG. 1. Contour plot over one period of the periodic part of the two-dimensional potential (a) Eq. (14) with $A_x - \Theta$, $A_y = \Theta$, $A_{xy} = -2\Theta$, $F_x = -0.1\Theta/L_x$, and $F_y = 0.6\Theta/L_y$; (b) Eq. (15) with $A_x = A_y = 0.5\Theta$, $A_{xy} = 3\Theta$, $F_x = -0.1\Theta/L_x$, $F_y = 0.6\Theta/L_y$, $A_1 = -1.9\Theta$, $\theta_1 = \pi/4$, $\sigma_{x1}^2 = 1/15$, $\sigma_{y1}^2 = 1/50$, $x_{o1} = y_{o1} = 0.7$, $A_2 = -1.25\Theta$, $\theta_2 = \pi/4$, $\sigma_{x2}^2 = 1/20$, $\sigma_{y2}^2 = 1/50$, and $x_{o2} = y_{o2} = 0.25$; (c) Eq. (18) with $A_{xy} = 3\Theta$, $F_x = F_y = 0$, and $U = 1.5$; and (d) Eq. (20) with $A_{xy} = 2\Theta$, $F_x = F_y = 0$, $U = 0.5$, $\theta_{1,2,5,6} = -7\pi/12$, $A_{1,5} = -2.5\Theta$, $\sigma_{x1,x5}^2 = 1/40$, $\sigma_{y1,y5}^2 = 1/50$, $x_{o1,o5} = 0.07$, $y_{o1,o5} = 0.20$, $A_{2,6} = -3.8\Theta$, $\sigma_{x2,x6}^2 = 1/35$, $\sigma_{x2,x6}^2 = 1/50$, $x_{o2,o6} = 0.19$, $y_{o2,o6} = 0.56$, $\theta_{3,4,7,8} = \pi/9$, $A_{3,7} = -2.5\Theta$, $\sigma_{x3,x7}^2 = 1/40$, $\sigma_{x3,x7}^2 = 1/50$, $x_{o3,o7} = 0.44$, $y_{o3,o7} = 0.81$, $A_{4,8} = -3.8\Theta$, $\sigma_{x4,x8}^2 = 1/35$, $\sigma_{y4,y8}^2 = 1/50$, $x_{o4,o8} = 0.80$, and $y_{o4,o8} = 0.93$. The colorbar corresponds to the depth of potential.

This potential contains separable and nonseparable terms and can exhibit narrow deep coupled channels along the diagonal when $A_{xy} \gg A_x, A_y$. The potential is shown for the example parameters in Fig. 1(a).

The second potential we consider has the form

$$V_{CG}(x, y) = V_{CC}(x, y) + \sum_{g=1}^{2} G_g(x, y; \theta_g), \quad (15)$$

where

$$G_g(x, y; \theta_g) = \sum_{\ell, J}^{\infty} A_g e^{-(\boldsymbol{r}-\boldsymbol{\mu}_{g\ell J})^T \boldsymbol{R}_{\theta_g}^T \boldsymbol{\sigma}_g \boldsymbol{R}_{\theta_g}(\boldsymbol{r}-\boldsymbol{\mu}_{g\ell J})}, \quad (16)$$

describes rotated elliptical Gaussian functions with matrices $\boldsymbol{R}_{\theta_g}$ and $\boldsymbol{\sigma}_g$ defined by

$$\boldsymbol{R}_{\theta_g} = \begin{pmatrix} \cos\theta_g & \sin\theta_g \\ \sin\theta_g & -\cos\theta_g \end{pmatrix}, \quad \boldsymbol{\sigma}_g = \begin{pmatrix} \frac{1}{L_x^2 \sigma_{xg}^2} & 0 \\ 0 & \frac{1}{L_y^2 \sigma_{yg}^2} \end{pmatrix}, \quad (17)$$

and the vector $\boldsymbol{r} - \boldsymbol{\mu}_{g\ell J} = (x - x_{og} - L_x\ell, y - y_{og} - L_y J)$, where ℓ, J are integers. Potential Eq. (15) has similar features to V_{CC} but it has additional metastable states per period due to the Gaussian functions Eq. (16). The potential is shown in Fig. 1(b).

We also consider two potentials that have a coupled channel taking a zigzag path through the landscape. The third

potential is

$$V_{ZZ}(x, y) = -A_{xy} \sin\left(2\pi\left[\frac{x}{L_x} - \frac{y}{L_y} + \frac{U}{2}f(x,y)\right]\right)$$
$$- F_x x - F_y y, \qquad (18)$$

where

$$f(x, y) = \sum_{p/\pi=1,3,5} \frac{4}{p^2} \cos\left(2p\left[\frac{x}{L_x} + \frac{y}{L_y}\right]\right). \qquad (19)$$

This potential displays tight coupling and is shown in Fig. 1(c).

Finally, we consider the potential

$$V_{ZG}(x, y) = V_{ZZ}(x, y) + \sum_{g=1}^{8} G_g(x, y; \theta_g), \qquad (20)$$

that has the same zigzag channel of potential V_{ZZ} but with the addition of metastable states along the coupled channel. This potential is shown in Fig. 1(d) and for certain parameters resembles the landscape proposed for ATP synthase [28,30]. For all model potentials considered in this paper we take the periodicity to be $L_x = L_y = L$.

We simulate stochastic single trajectories for the two-dimensional model potentials using Eq. (3). The trajectories have duration τ and sampling frequency f_s. The steady-state probability density $P(x, y)$ is then approximated from the simulated trajectories by building a two-dimensional position histogram within a single period [35]. The position histogram has N_b bins in each dimension so the total number of bins is N_b^2. Figure 2(a) shows an example trajectory for the simple potential Eq. (14). The steady-state probability density $P(x, y)$ in one period approximated from the trajectory is shown in Fig. 2(b). Note that the full two-dimensional steady-state probability density is recovered from the full two-dimensional simulated trajectory.

The free-energy potential landscape is reconstructed from the approximate steady-state probability density using the multidimensional k-space method described in Sec. II B. The periodic part of the reconstructed potential in k space is $V_{\boldsymbol{k}}^{\boldsymbol{0}}$, where $\boldsymbol{k} = (k_x, k_y)$. The terms along the axes with either $k_x = 0$ or $k_y = 0$ are due to the separable parts of the potential, but there are also terms with $k_x \neq 0$ and $k_y \neq 0$ due to the nonseparable coupling terms. Figure 3 shows an example of a nonseparable reconstructed potential in k space.

Figure 4 show examples of the landscape reconstruction for the model potentials. In all cases we find that the reconstructed potentials determined via the k-space method from simulated single trajectories are in qualitative agreement with the original model potentials.

To quantitatively determine the accuracy of the landscape reconstruction, confidence intervals are not an appropriate measure because they do not propagate linearly in the k-space inversion of the probability density to the reconstructed potential [35]. Instead, we measure the overall accuracy of the reconstruction method using the mean-squared error $\mathrm{MSE}_{\mathrm{pot}}$ between the original potential and its reconstruction from
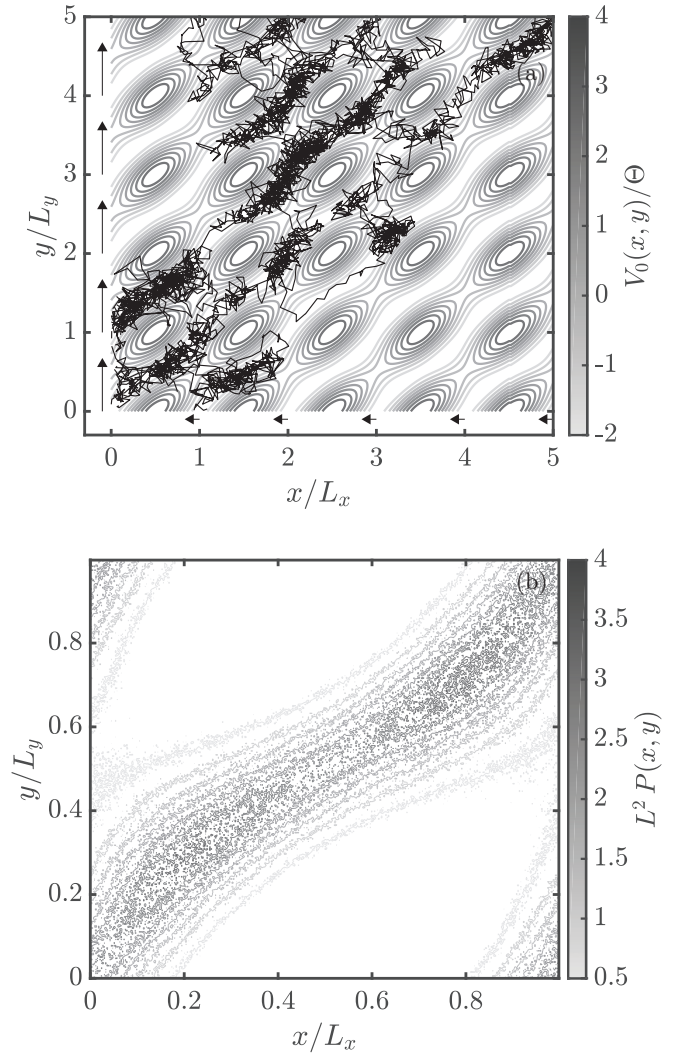
FIG. 2. (a) Single-trajectory simulated using the Langevin equation (3) for the two-dimensional potential Eq. (14) mapped over the contour plot of the periodic part of the potential with black arrows indicating the direction and relative magnitude of the force $\boldsymbol{F}$. (b) Approximate steady-state probability density $P(x, y)$ computed from the trajectory in (a) via a position histogram. Potential parameters are $A_x = -\Theta$, $A_y = \Theta$, $A_{x,y} = -2\Theta$, $F_x = -0.1\Theta/L_x$, and $F_y = 0.6\Theta/L_y$. Trajectory parameters are $\tau\Theta/\gamma L^2 = 100$, $\gamma L^2 f_s/\Theta = 7.0 \times 10^4$, and $N_b = 1000$.

trajectories, i.e., we define

$$\mathrm{MSE}_{\mathrm{pot}} = \frac{1}{N_b^2} \sum_{i=1}^{N_b} \sum_{j=1}^{N_b} \left[V_{i,j} - V_{i,j}^{\mathrm{R}}\right]^2, \qquad (21)$$

where $V_{i,j}$ and $V_{i,j}^{\mathrm{R}}$ are the original and reconstructed potentials, respectively, evaluated at the center of the bins used in the position histogram approximation of the steady-state probability density [35]. The mean-squared error for the reconstructions shown in Fig. 4 are provided in the figure caption.

An analysis of the convergence of the $\mathrm{MSE}_{\mathrm{pot}}$ value was carried out, similarly to that provided for one-dimensional systems in Refs. [34,35]. In general, we observed the same
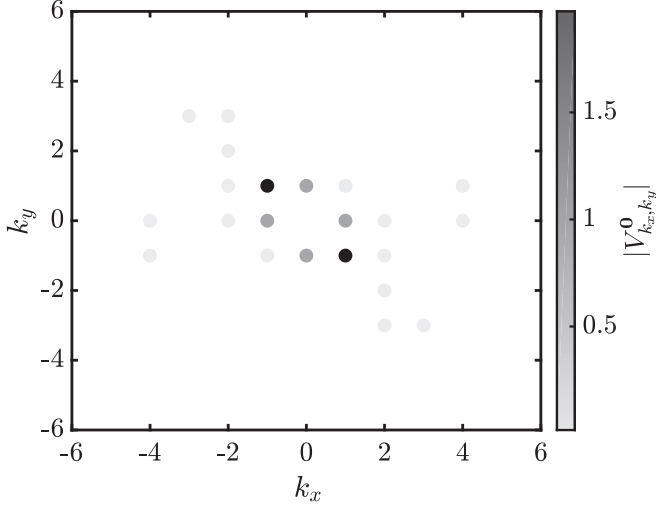
FIG. 3. Fourier coefficients $V_{\boldsymbol{k}}^{\boldsymbol{0}}$ for the reconstructed potential Eq. (14) with parameters $A_x = -\Theta$, $A_y = \Theta$, $A_{xy} = -2\Theta$, and $\boldsymbol{F} = \boldsymbol{0}$. Trajectory parameters are $\mathcal{K} = 21$, $\tau\Theta/\gamma L^2 = 100$, and $\gamma L^2 f_s/\Theta = 7.0 \times 10^4$, and $N_b = 1000$. Terms with $k_{x,y} > \pm 6$ are not shown because $|V_{\boldsymbol{k}}^{\boldsymbol{0}}| < 10^{-13}$.

trends in two dimensions as for landscape reconstructions in one dimension, i.e., convergence for increasing number of Fourier terms $\mathcal{K}$, increasing trajectory duration τ, and increasing sampling frequency f_s [35]. An example of the convergence with the number of Fourier terms $\mathcal{K}$ is shown in Fig. 5. In this case we determined the steady-state probability density $P(x, y)$ numerically from the Smoluchowski equation (1)
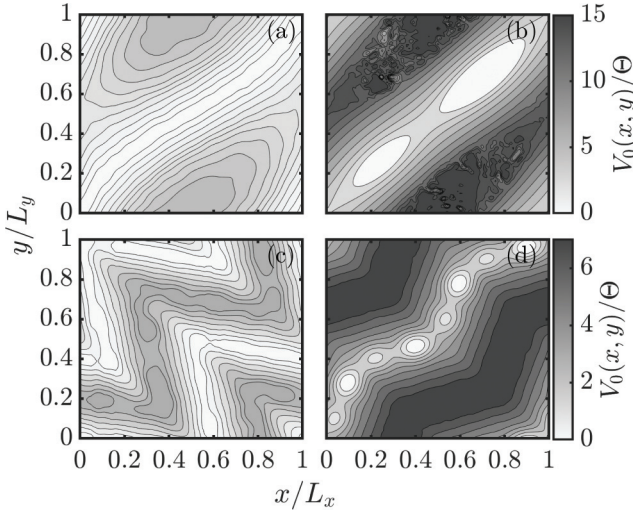
FIG. 4. Full two-dimensional landscape reconstruction from trajectories, showing (a) Eq. (14), (b) Eq. (15), (c) Eq. (18), and (d) Eq. (20). Potential parameters used same as in Fig. 1. Trajectories parameters: (a) $\tau\Theta/\gamma L^2 = 100$, $\gamma L^2 f_s/\Theta = 7.0 \times 10^4$; (b) $\tau\Theta/\gamma L^2 = 100$, $\gamma L^2 f_s/\Theta = 1.2 \times 10^4$; (c) $\tau\Theta/\gamma L^2 = 100$, $\gamma L^2 f_s/\Theta = 1.0 \times 10^4$; and (d) $\tau\Theta/\gamma L^2 = 1000$, $\gamma L^2 f_s/\Theta = 1.4 \times 10^5$. Mean-squared errors: (a) $\text{MSE}_{\text{pot}} = 0.018$, $\mathcal{K} = 21$ and $N_b = 1000$; (b) $\text{MSE}_{\text{pot}} = 0.0475$, $\mathcal{K} = 61$ and $N_b = 1000$; (c) $\text{MSE}_{\text{pot}} = 0.015$, $\mathcal{K} = 31$ and $N_b = 1000$; (d) $\text{MSE}_{\text{pot}} = 8.3 \times 10^{-4}$, $\mathcal{K} = 61$ and $N_b = 1000$.
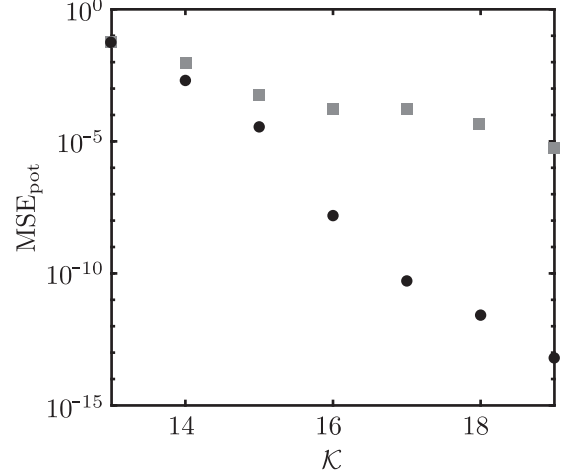
FIG. 5. Mean-squared error MSE_{pot} for the two-dimensional landscape reconstruction of potential Eq. (14) with increasing Fourier terms $\mathcal{K}$ and (dots) direct inversion with known force and (squares) iterative inversion with unknown force. The probability density $P(x, y)$ is determined by numerically solving the Smoluchowski equation (1) for V_{cc} with potential parameters the same as in Fig. 2.

and determined the accuracy of the k-space inversion for both direct reconstruction where $\boldsymbol{F}$ is known and iterative reconstruction where $\boldsymbol{F}$ is not known but drift $\boldsymbol{v}$ is known. The convergence with τ and f_s is shown in Fig. 6. In this case the probability density was built from simulated single trajectories and the force was assumed to be known. Finally, Table I provides a guide to the accuracy that can be expected for one- and two-dimensional cosinelike potentials with barrier heights in the range Θ to 7Θ.
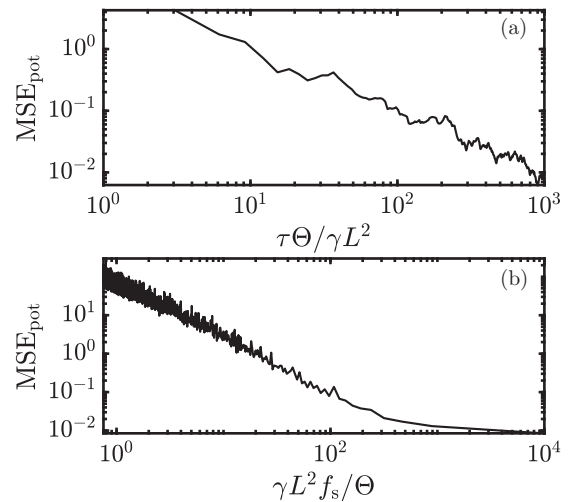
FIG. 6. Mean-squared error MSE_{pot} for the two-dimensional landscape reconstruction of potential Eq. (20) with (a) increasing trajectory duration τ at fixed sampling frequency $\gamma L^2 f_s/\Theta = 10^4$ and (b) increasing sampling frequency f_s at fixed trajectory duration $\tau\Theta/\gamma L^2 = 1000$. The force $\boldsymbol{F}$ is known, $\mathcal{K} = 61$, $N_b = 1000$, and the potential parameters are the same as in Fig. 4(c).

TABLE I. Expected mean-squared error MSE$_{pot}$ for reconstructed one- and two-dimensional cosinelike potentials with the trajectory duration τ and sampling frequency f_s required to achieve that level of accuracy. †In two dimensions, N_b is the number of grid points in each direction so the total number of bins is N_b^2.

	MSE$_{pot}$	$\tau \, \Theta/\gamma L^2$	$\gamma L^2 f_s/\Theta$	N_b
1D known force	$\sim 10^{-4}$	$\sim 10^2$	$\sim 10^4$	100
1D unknown force	$\sim 10^{-2}$	$\sim 10^2$	$\sim 10^4$	100
2D known force	$\sim 10^{-2}$	$\sim 10^3$	$\sim 10^4$	$1000^\dagger$
2D unknown force	$\sim 10^{-1}$	$\sim 10^3$	$\sim 10^4$	$1000^\dagger$

IV. EFFECTIVE DYNAMICS PROJECTED ON ONE DIMENSION

In this section we explore the implications of only measuring one degree of freedom. To make the discussion concrete we consider a mechanochemical molecular motor with one mechanical and one chemical degree of freedom. Most motor proteins with unidirectional mechanical motion [8,39,40] are expected to be well described by this treatment assuming the proper chemical reaction coordinate [43,44]. We take x to be the measured mechanical degree of freedom and y to be the unmeasured chemical degree of freedom. Our aim is to establish the connection between the full two-dimensional dynamics and the effective projected dynamics on the mechanical degree of freedom and determine the implications of this for landscape reconstruction and elucidating energy conversion.

A. Effective one-dimensional potential

We consider that only the mechanical degree of freedom x is measured and define the effective one-dimensional projected probability density

$$P^{\text{RX}}(x) = \int_0^{L_y} dy \, P(x, y). \quad (22)$$

Expanding the two-dimensional probability density $P(x, y)$ in its Fourier series according to Eq. (8) and using the definition of the reduced density Eq. (22) yields

$$P^{\text{RX}}(x) = L_y \sum_{k_x} P_{k_x,0} \, e^{i2\pi k_x x/L_x}. \quad (23)$$

This shows that $P^{\text{RX}}(x)$ is periodic.

We now show that it is always possible to reconstruct an effective tilted periodic potential $V^{\text{eff}}(x) = V_0^{\text{eff}}(x) - F_x^{\text{eff}}x$ from the probability density $P^{\text{RX}}(x)$ and we derive an analytic expression for the effective one-dimensional potential from the two-dimensional potential. First, assuming the effective one-dimensional potential exists, we write the effective one-dimensional steady-state Smoluchowski equation,

$$0 = \frac{1}{\gamma} \frac{\partial}{\partial x} \left[\Theta \frac{\partial}{\partial x} + \frac{\partial V^{\text{eff}}(x)}{\partial x} \right] P^{\text{RX}}(x). \quad (24)$$

Integrating the two-dimensional steady-state Smoluchowski equation over the chemical degree of freedom we have

$$0 = \int_0^{L_y} dy \sum_j \frac{1}{\gamma_j} \frac{\partial}{\partial r_j} \left[\Theta \frac{\partial}{\partial r_j} + \frac{\partial V(x, y)}{\partial r_j} \right] P(x, y)$$

$$= \frac{\Theta}{\gamma} \frac{\partial^2}{\partial x^2} \int_0^{L_y} dy \, P(x, y) + \frac{1}{\gamma} \frac{\partial}{\partial x} \int_0^{L_y} dy \frac{\partial V(x, y)}{\partial x} P(x, y). \quad (25)$$

Comparing Eqs. (24) and (25) we find that the effective one-dimensional potential can be written

$$V^{\text{eff}}(x) = \int_0^x \frac{dx'}{P^{\text{RX}}(x')} \int_0^{L_y} dy \, P(x', y) \frac{\partial V(x', y)}{\partial x'}. \quad (26)$$

When the potential is separable, we have $V(x, y) = \mathcal{V}_{0x}(x) + \mathcal{V}_{0y}(y) - F_x x - F_y y$ and Eq. (26) reduces to

$$V^{\text{eff}}(x) = \int_0^x dx' \frac{\partial V(x', y)}{\partial x'} = \mathcal{V}_{0x}(x) - F_x x, \quad (27)$$

where we have taken $\mathcal{V}_{0x}(0) = 0$ without loss of generality. Equation (27) shows that for a separable potential the effective one-dimensional potential is the original x component of the full two-dimensional potential, i.e., $V_0^{\text{eff}}(x) = \mathcal{V}_{0x}(x)$ and $F_x^{\text{eff}} = F_x$.

In general, for nonseparable potentials, we define the auxiliary function

$$\varrho(x') = \frac{1}{P^{\text{RX}}(x')} = \sum_s \varrho_s e^{i2\pi s x'/L_x}, \quad (28)$$

which is also periodic. Substituting Eq. (28) into the effective potential Eq. (26) gives

$$V^{\text{eff}}(x) = \int_0^x dx' \varrho(x') \int_0^{L_y} dy \, P(x', y) \frac{\partial}{\partial x'} V(x', y). \quad (29)$$

Using $V(x, y) = V_0(x, y) - F_x x - F_y y$ and the corresponding Fourier expansions for $\varrho(x)$, $P(x, y)$, and $V_0(x, y)$, we find formal expressions for F_x^{eff} and $V_0^{\text{eff}}(x)$. This yields the effective force

$$F_x^{\text{eff}} = F_x - i2\pi \frac{L_y}{L_x} \sum_{\boldsymbol{k}, q_x} q_x \varrho_{-(k_x+q_x)} P_{k_x,k_y} V^{\mathbf{0}}_{q_x,-k_y}, \quad (30)$$

and the effective one-dimensional periodic potential

$$V_0^{\text{eff}}(x) = L_y \sum_{\boldsymbol{k}, q_x, s \neq -k_x - q_x} \left(\frac{q_x \varrho_s P_{k_x,k_y} V^{\mathbf{0}}_{q_x,-k_y}}{s + k_x + q_x} \right)$$
$$\times [e^{i2\pi(s+k_x+q_x)x/L_x} - 1]. \quad (31)$$

Equations (30) and (31) relate the two-dimensional nonseparable tilted periodic potential with the effective one-dimensional tilted periodic potential projected on the mechanical degree of freedom.

Equation (30) shows that in general F_x^{eff} has two terms, a linear dependence on F_x that is expected for a separable potential, as well as an additional term that depends on the nonseparable periodic potential $V_0(x, y)$ and the force $\boldsymbol{F}$ via the probability density $P(x, y)$ and $\varrho(x)$. In Fig. 7 we show the dependence of F_x^{eff} on a range of forces $\boldsymbol{F}$ for different
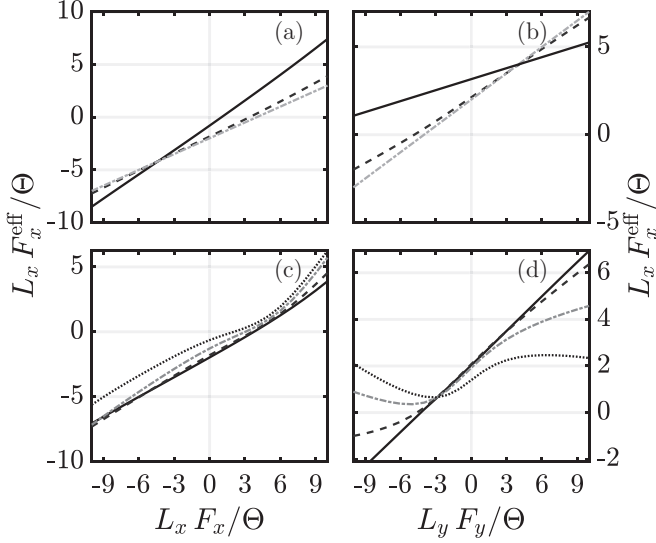
FIG. 7. Effective force F_x^{eff} as a function of [(a) and (c)] force F_x for $F_y = -4\Theta/L_y$ and [(b) and (d)] force F_y for $F_x = 4\Theta/L_x$. [(a) and (b)] The potential is Eq. (14) with (solid) $A_x = -2\Theta$, $A_y = 2\Theta$, $A_{xy} = -2\Theta$, (dashed) $A_x = -2\Theta$, $A_y = 2\Theta$, $A_{xy} = -4\Theta$, and (dash-dotted) $A_x = A_y = 0$ and $A_{xy} = -8\Theta$. [(c) and (d)] The potential is Eq. (18) with $A_{xy} = 4\Theta$ and (solid) $U = 0$, (dashed) $U = 0.5$, (dash-dotted) $U = 1$, and (dotted) $U = 1.5$.

potentials. For cosinelike potentials of the form Eq. (14), the relation between the forces F_x and F_y and the effective force F_x^{eff} is linear, as seen in Figs. 7(a) and 7(b). For potentials of the form Eq. (18), the relation is nonlinear, as shown in Figs. 7(c) and 7(d). For convenience in this section, all numerical calculations are based on the probability density $P(x, y)$ determined by directly solving the Smoluchowski equation (1). We also assume that the force $\boldsymbol{F}$ is known.

Not only does the effective force F_x^{eff} depend on both F_x and F_y, but also the periodic part of the effective one-dimensional potential depends on both F_x and F_y. This is shown in Eq. (31) where the effective one-dimensional potential depends on the force $\boldsymbol{F}$ through the probability density $P(x, y)$ and $\varrho(x)$. This is important because, for nonseparable potentials, $V_0^{\text{eff}}(x)$ is no longer a function of solely the mechanical coordinate but is different for different external forces. Examples of reconstructed effective one-dimensional potentials $V_0^{\text{eff}}(x)$ are shown in Fig. 8 for [Fig. 8(a)] six different values of the force F_x at fixed F_y and [Fig. 8(b)] for variable F_y at fixed F_x. The effective forces F_x^{eff} for each of the cases are given in Table II. We find that not only varying the mechanical force affects the effective periodic potential but, because of the nonseparability of the potential, varying the chemical force also affects the periodic part of the effective one-dimensional potential.

B. Signatures of energy coupling

In the previous section we determined the relationship between a full nonseparable two-dimensional landscape and its corresponding effective one-dimensional potential projected on one degree of freedom. This brings into question what can be determined about the system from
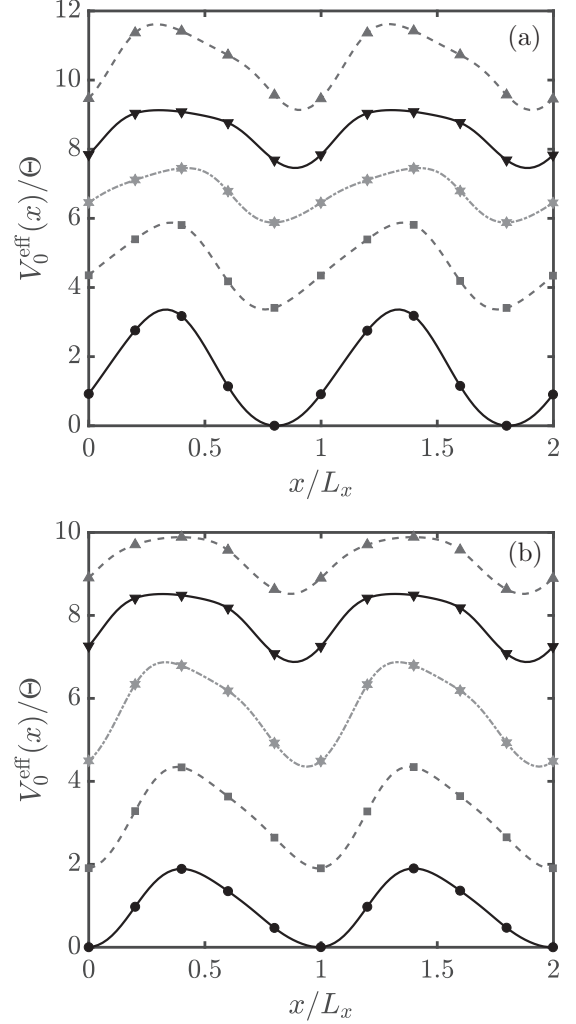
FIG. 8. Effective one-dimensional periodic potential $V_0^{\text{eff}}(x)$ for (a) fixed $F_y = 6\Theta/L_y$ and (dots) $F_x = -10\Theta/L_x$, (squares) $F_x = -5\Theta/L_x$, (hexagrams) $F_x = 0\Theta/L_x$, (down-triangles) $F_x = 5\Theta/L_x$, and (up-triangles) $F_x = 10\Theta/L_x$ and (b) fixed $F_x = 4\Theta/L_x$ with (dots) $F_y = -10\Theta/L_y$, (squares) $F_y = -5\Theta/L_y$, (hexagrams) $F_y = 0\Theta/L_y$, (down-triangles) $F_y = 5\Theta/L_y$, and (up-triangles) $F_y = 10\Theta/L_y$. In all cases the two-dimensional potential is Eq. (18) with $A_{xy} = 3\Theta$ and $U = 1.5$.

TABLE II. Force $\boldsymbol{F}$ and calculated effective force F_x^{eff} for the cases shown in Fig. 8.

$L_x F_x/\Theta$,	$L_y F_y/\Theta$	$L_x F_x^{\text{eff}}/\Theta$
-10	6	-7.9
-5	6	-3.0
0	6	0.3
5	6	3.1
10	6	6.6
4	-10	3.2
4	-5	1.9
4	0	1.8
4	5	2.5
4	10	2.4
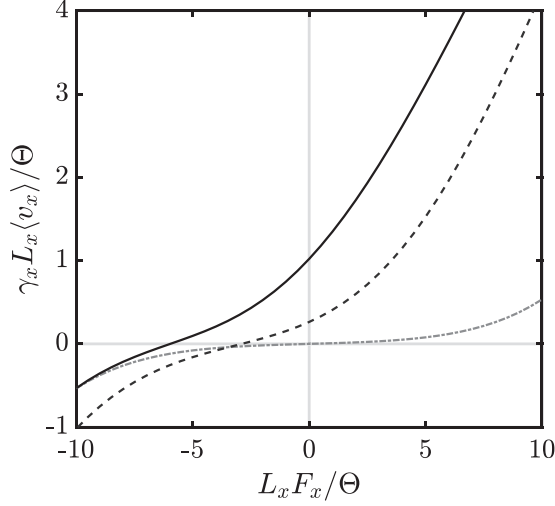
FIG. 9. Drift velocity with force in the mechanical degree of freedom for potential Eq. (14) with $F_y = 6\Theta/L_y$ and (solid) $A_x = -3\Theta$, $A_y = 1\Theta$, $A_{x,y} = -6\Theta$; (dashed) $A_x = -4\Theta$, $A_y = 2\Theta$, $A_{x,y} = -3\Theta$; and (dash-dotted) $A_x = -4\Theta$, $A_y = 1\Theta$, and $A_{x,y} = 0$.

the effective one-dimensional potential alone, not knowing the full two-dimensional landscape. In this section, we identify signatures of energy conversion in the effective one-dimensional dynamics.

For a one-dimensional system with $r = x$, the steady-state drift velocity Eq. (5) has the closed analytic solution [32,45–47]

$$\langle v \rangle = \frac{1 - e^{-FL/\Theta}}{\gamma N/\Theta L}, \tag{32}$$

where N is the normalization constant of the steady-state probability density over one period. From this equation it is possible to show that (i) the drift velocity $\langle v \rangle$ is zero at zero force F, (ii) the force and drift velocity have the same sign, and (iii) the drift velocity is a monotonic function of the force [48].

Equation (32) and the properties (i)–(iii) also hold for each degree of freedom in the case of a separable potential. Thus, in two dimensions, if the velocity-force relation in the mechanical degree of freedom does not satisfy all of the properties (i)–(iii) above then this suggests the presence of a nonseparable potential and coupling with another degree of freedom.

Using the model two-dimensional potentials Eq. (14) and Eq. (18), we determined the drifts $\langle v_x \rangle$ and $\langle v_y \rangle$ from Eq. (5). The results are shown in Figs. 9 and 10 for a range of forces F_x and a fixed value of F_y. Figure 9 shows that for a (dash-dotted) separable potential all the properties (i)–(iii) are satisfied. However, for a nonseparable potential the drift is nonzero at finite force, violating property (i). Moreover, there is a region where $\langle v_x \rangle > 0$ for $F_x < 0$, violating property (ii) and demonstrating energy coupling in the system (see Sec. II A). In addition, increasing the coupling strength increases the drift velocity at $F_x = 0$. These results are in accordance with experimental observations measuring the maximum torque exerted by rotatory molecular motors [15,49] and support the standard interpretation that the nonzero interceptor of the drift
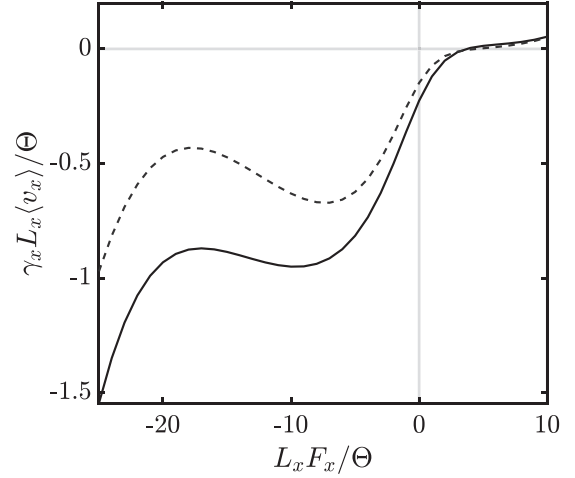
FIG. 10. Drift velocity with force in the mechanical degree of freedom for potential Eq. (18) with $F_y = -4\Theta/L_y$, $A_{x,y} = 6\Theta$, and (solid) $U = 1.5$ and (dashed) $U = 1.8$.

velocity is due to the driving chemical degree of freedom (in our formalism represented by $F_y > 0$). Figure 9 also shows that the degree of coupling increases the force required to achieve zero drift. Figure 10 shows that for certain geometries of the coupling channel, the velocity-force relation becomes nonmonotonic, violating property (iii).

So far in Sec. IV we have assumed that the force $\boldsymbol{F}$ is known. However, in the case that $\boldsymbol{F}$ is not known, it is no longer possible to determine the relation between the steady-state drift and the force $\boldsymbol{F}$. Instead, we can use the iterative reconstruction method in one-dimension with the measured drift velocity $\langle v_x \rangle$ [34,35] to determine the effective one-dimensional potential $V^{\text{eff}}(x)$. The relation between the steady-state drift $\langle v_x \rangle$ and the effective force F_x^{eff} satisfies Eq. (32) and properties (i)–(iii), so to identify coupling to another degree of freedom we must reconstruct the periodic part of the effective one-dimensional potential for different forces $\boldsymbol{F}$. As shown in Eq. (31) and Fig. 8, when the two-dimensional potential is nonseparable, different effective periodic potentials $V_0^{\text{eff}}(x)$ are obtained for different forces. Similar ideas of chemical force dependent potentials have been recently proposed elsewhere [50].

C. Tight-coupling regime

In this section we consider under what circumstances the effective one-dimensional potential $V_0^{\text{eff}}(x)$ can be used to infer features of the full two-dimensional potential. From our survey of the model potentials, we find that this is usually only possible when the two degrees of freedom are tightly coupled and when the path of the deep channel in the landscape is along the diagonal. For this discussion we focus on the potentials $V_{\text{CG}}(x, y)$ and $V_{\text{ZG}}(x, y)$ that display metastable states along the coupled channel.

In the tight-coupling regime, the nonseparable part of the potential dominates and the two-dimensional landscape exhibits a deep narrow coupled channel. In this case the probability density $P(x, y)$ is tightly confined to the channel. We numerically solve the Smoluchowski equation for
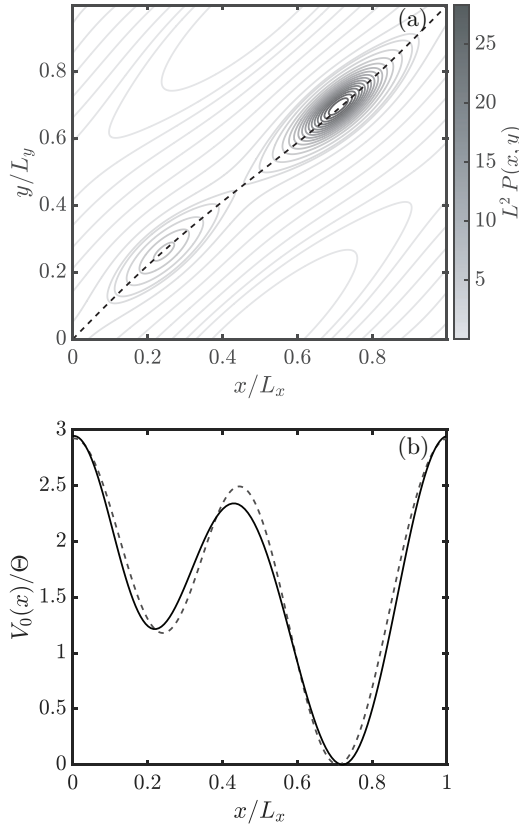
FIG. 11. (a) Contour plot of the two-dimensional steady-state probability density $P(x, y)$ with (dashed) the minimum energy path of the coupled channel. (b) (dashed) Reconstructed effective one-dimensional potential $V_0^{\text{eff}}(x)$ and (solid) two-dimensional potential along the channel path projected onto the x axis V_0^s. The potential is Eq. (15) in the tight-coupling regime with the parameters the same as in Fig. 1(d).

FIG. 12. (a) Contour plot of the two-dimensional steady-state probability density $P(x, y)$ with (dashed) the minimum energy path of the coupled channel. (b) (dashed) Reconstructed effective one-dimensional potential $V_0^{\text{eff}}(x)$ and (solid) two-dimensional potential along the channel path projected onto the x axis V_0^s. The potential is Eq. (20) in the tight-coupling regime with the parameters the same as in Fig. 1(d).

the two-dimensional probability density and then calculate $P^{\text{RX}}(x)$ using Eq. (23). Then we reconstruct the effective one-dimensional potential $V^{\text{eff}}(x)$ from the effective probability density $P^{\text{RX}}(x)$. The effective potential is then compared with the two-dimensional potential along the minimum energy path of the coupled channel projected onto the x axis $V^s(x)$. This comparison is only possible because we know the model two-dimensional potential and the path of the channel in two dimensions $\{x(s), y(s)\}$. Typically, when reconstructing potentials from single trajectory data, the underlying two-dimensional landscape would not be known so the results presented in this section are for illustrative purposes only.

Figure 11 shows the two-dimensional probability density and reconstructed effective one-dimensional potential for the diagonal potential $V_{\text{CG}}(x, y)$ Eq. (15). We find good agreement between the reconstructed effective one-dimensional potential and the two-dimensional potential along the channel shown as the dashed line in Fig. 11(a).

In contrast, Fig. 12 shows the analogous calculation for the zigzaglike potential Eq. (18). In this case the reconstructed effective one-dimensional potential and the projected channel of the two-dimensional landscape are very different. We can understand this by noting that as the system moves along the channel it spends significant time at certain regions of x while

moving along the y direction. Although not within a single minimum of the two-dimensional potential during this time, if only the x degree of freedom is measured, this behavior leads to a deep minimum in the reconstructed effective one-dimensional potential. Therefore, despite knowing the path of the coupled channel, the reconstructed potential $V^{\text{eff}}(x)$ does not accurately predict the profile of the two-dimensional landscape along the channel. In this case, the reconstructed effective one-dimensional potential is of limited value for understanding the features of the full two-dimensional free-energy landscape and full two-dimensional dynamic information is needed to reconstruct the two-dimensional landscape.

V. SUMMARY

We have presented a k-space method for reconstructing multidimensional free-energy potential landscapes of cyclic molecular motors from stochastic single trajectories. Using a range of model potentials in two dimensions we have demonstrated that full two-dimensional stochastic trajectories can be used to reconstruct full two-dimensional free-energy

landscapes. When the external force is known in both degrees of freedom, the landscape can be reconstructed directly from the probability density and the Fourier decomposition of the reconstructed potential enables mechanochemical coupling in the system to be identified. If the external force is not known in one or both degrees of freedom, then the steady-state drift velocity can be used in an iterative method to reconstruct the two-dimensional potential landscape, determine the forces on the system, and identify mechanochemical coupling. As in the one-dimensional case [34,35], we found the reconstruction method to be robust in two dimensions with convergence for increasing duration and sampling frequency of trajectories.

We also considered the case where the multidimensional system is measured in only one degree of freedom. For mechanochemical systems, it is always possible to reconstruct an effective one-dimensional tilted periodic potential from the effective one-dimensional probability density projected onto the mechanical degree of freedom. The reconstructed effective one-dimensional potential depends on the full two-dimensional potential, including the external forces in both the mechanical and chemical degrees of freedom. In general, the effective one-dimensional potential cannot be used to understand the features of the full underlying two-dimensional landscape. However, even with dynamic information in only one dimension it is possible to identify signatures of energy conversion. If the external forces on the system are known, then nonseparability and energy coupling can be identified by reconstructing the effective one-dimensional potential and examining the drift-force relation in the observed degree of freedom. If the external forces on the system are not known, coupling can be identified by reconstructing the effective one-dimensional potential for a range of forces and observing a force dependence in the periodic part of the effective one-dimensional potential.

This work highlights three key messages for experimental studies of molecular motors. (1) It is often not obvious how many degrees of freedom are needed for describing a system, but by reconstructing an effective potential along one degree of freedom and analyzing the drift-force relation and/or the force dependence of the reconstructed effective one-dimensional potential it is possible to differentiate between a purely one-dimensional system and an effective one-dimensional system with hidden coupled degrees of freedom. (2) In general, the effective one-dimensional potential reconstructed from single trajectories measured in only one degree of freedom is force dependent. This means that for mechanochemical molecular motors, different chemical force regimes can lead to different barrier heights in the reconstructed effective one-dimensional potential in the mechanical degree of freedom. Therefore, it is necessary to obtain experimental measurements for a wide range of forces to better understand the coupling dynamics of the system. (3) Typically in current experiments only one mechanical degree of freedom is measured with single-molecule resolution. However, the effective potential reconstructed in one degree of freedom is only indicative of the features of the full two-dimensional potential for tightly coupled systems with a diagonal path on the landscape. Being unable to simultaneous measure both mechanical and chemical degrees of freedom is a significant handicap in understanding the full two-dimensional free-energy landscape and elucidating energy coupling. Achieving simultaneous measurement of multiple degrees of freedom may be more realistic in systems with two mechanical degrees of freedom. Alternative systems to consider would be electromechanical artificial molecular machines [51–54] or ion gradient pumps in lipid membranes [11].

In this paper we have assumed that the potential landscape is tilted periodic in all relevant degrees of freedom. However, it is possible that one or more of the degrees of freedom may be confined [48]. Provided the potential landscape of the system is nonseparable we would still expect effects similar to those described here, although the k-space method would need to be modified in this case. We have also only considered equal periodicity and equal viscous drag coefficients in all degrees of freedom. It would be interesting to consider systems with very different dynamic timescales between different degrees of freedom [55–57].

ACKNOWLEDGMENTS

[1] J. N. Onuchic, Z. Luthey-Schulten, and P. G. Wolynes, Annu. Rev. Phys. Chem. **48**, 545 (1997).

[2] G. Hummer and A. Szabo, Proc. Natl. Acad. Sci. USA **98**, 3658 (2001).

[3] N. C. Harris, Y. Song, and C.-H. Kiang, Phys. Rev. Lett. **99**, 068101 (2007).

[4] G. G. Maisuradze, A. Liwo, and H. A. Scheraga, J. Chem. Theory Comput. **6**, 583 (2010).

[5] M. de Messieres, B. Brawn-Cinani, and A. La Porta, Biophys. J. **100**, 2736 (2011).

[6] A. N. Gupta, A. Vincent, K. Neupane, H. Yu, F. Wang, and M. T. Woodside, Nat. Phys. **7**, 631 (2011).

[7] H. Yu, A. N. Gupta, X. Liu, K. Neupane, A. M. Brigley, I. Sosova, and M. T. Woodside, Proc. Natl. Acad. Sci. USA **109**, 14452 (2012).

[8] M. Hinczewski, J. C. M. Gebhardt, M. Rief, and D. Thirumalai, Proc. Natl. Acad. Sci. USA **110**, 4500 (2013).

[9] N. P. Schafer, B. L. Kim, W. Zheng, and P. G. Wolynes, Isr. J. Chem. **54**, 1311 (2014).

[10] M. T. Woodside and S. M. Block, Annu. Rev. Biophys. **43**, 19 (2014).

[11] R. D. Astumian and I. Derényi, Eur. Biophys. J. **27**, 474 (1998).

[12] C. Bustamante, D. Keller, and G. Oster, Acc. Chem. Res. **34**, 412 (2001).

[13] R. D. Astumian, Appl. Phys. A **75**, 193 (2002).

[14] R. D. Astumian, Biophys. J. **98**, 2401 (2010).

[15] S. Toyabe, T. Watanabe-Nakayama, T. Okamoto, S. Kudo, and E. Muneyuika, Proc. Natl. Acad. Sci. USA **108**, 17951 (2011).

[16] K. Kinosita-Jr., R. Yasuda, H. Noji, and K. Adachi, Philos. Trans. R. Soc. London B **355**, 473 (2000).

[17] Y. Hirono-Hara, K. Ishizuka, J. Kazuhiko Kinosita, M. Yoshida, and H. Noji, Proc. Natl. Acad. Sci. USA **102**, 4288 (2005).

[18] J. Xing, F. Bai, R. Berry, and G. Oster, Proc. Natl. Acad. Sci. USA **103**, 1260 (2006).

[19] E. Gerritsma and P. Gaspard, Biophys. Rev. Lett. **05**, 163 (2010).

[20] D. Boyer and D. S. Dean, J. Phys. A: Math. Theor. **44**, 335003 (2011).

[21] R. Watanabe, D. Okuno, S. Sakakihara, K. Shimabukuro, R. Iino, M. Yoshida, and H. Noji, Nat. Chem. Biol. **8**, 86 (2012).

[22] R. Hayashi, K. Sasaki, S. Nakamura, S. Kudo, Y. Inoue, H. Noji, and K. Hayashi, Phys. Rev. Lett. **114**, 248101 (2015).

[23] R. Yasuda, H. Miyata, and J. Kazuhiko Kinosita, J. Mol. Biol. **263**, 227 (1996).

[24] O. Pänke, D. A. Cherepanov, K. Gumbiowski, S. Engelbrecht, and W. Junge, Biophys. J. **81**, 1220 (2001).

[25] M. Lindén and M. Wallin, Biophys. J. **92**, 3804 (2007).

[26] R. Watanabe and H. Noji, Nat. Commun. **5**, 3486 (2014).

[27] D. Wales, *Energy Landscapes* (Cambridge University Press, Cambridge, 2003).

[28] S. Mukherjee and A. Warshel, Proc. Natl. Acad. Sci. USA **109**, 14876 (2012).

[29] S. Mukherjee, R. Alhadeff, and A. Warshel, Proc. Natl. Acad. Sci. USA **114**, 2259 (2017).

[30] S. Mukherjee and A. Warshel, Photosynth. Res. **134**, 1 (2017).

[31] H. Wang, J. Theor. Biol. **242**, 908 (2006).

[32] J. Wedekind and D. Reguera, J. Phys. Chem. B **112**, 11060 (2008).

[33] Q. Zhang, J. Brujić, and E. Vanden-Eijnden, J. Stats. Phys. **144**, 344 (2011).

[34] N. J. López-Alamilla, M. W. Jack, and K. J. Challis, Phys. Rev. E **97**, 032419 (2018).

[35] N. J. López-Alamilla, M. W. Jack, and K. J. Challis, J. Theor. Biol. **462**, 321 (2019).

[36] M. O. Magnasco, Phys. Rev. Lett. **72**, 2656 (1994).

[37] D. Keller and C. Bustamante, Biophys. J. **78**, 541 (2000).

[38] K. J. Challis and M. W. Jack, Phys. Rev. E **88**, 042114 (2013).

[39] K. Svoboda and S. M. Block, Cell **77**, 773 (1994).

[40] S. Toyabe, H. Ueno, and E. Muneyuki, Europhys. Lett. **97**, 40004 (2012).

[41] C. W. Gardiner, *Handbook of Stochastic Methods for Physics, Chemistry and the Natural Sciences* (Springer, Berlin, 1985).

[42] M. W. Jack and C. Tumlin, Phys. Rev. E **93**, 052109 (2016).

[43] H. Kramers, Physica **7**, 284 (1940).

[44] P. Hänggi, P. Talkner, and M. Borkovec, Rev. Mod. Phys. **62**, 251 (1990).

[45] H. Risken, *The Fokker-Planck Equation* (Springer, Berlin, 1989).

[46] P. Reimann, C. Van den Broeck, H. Linke, P. Hänggi, J. M. Rubi, and A. Pérez-Madrid, Phys. Rev. Lett. **87**, 010602 (2001).

[47] R. L. Stratonovich, Radiotekh Elektr. (Moscow) **3**, 497 (1958).

[48] G. A. Cecchi and M. O. Magnasco, Phys. Rev. Lett. **76**, 1968 (1996).

[49] R. Shinagawa and K. Sasaki, J. Phys. Soc. Jpn. **85**, 064004 (2016).

[50] R. D. Astumian, S. Mukherjee, and A. Warshel, ChemPhysChem **17**, 1719 (2016).

[51] T. F. Otero and J. Rodriguez, Electrochemomechanical and electrochemopositioning devices: Artificial muscles, in *Intrinsically Conducting Polymers: An Emerging Technology*, edited by M. Aldissi (Springer, The Netherlands, 1993), pp. 179–190.

[52] R. A. Bissell, E. Córdova, A. E. Kaifer, and J. F. Stoddart, Nature **369**, 133 (1994).

[53] J.-P. Sauvage, Acc. Chem. Res. **31**, 611 (1998).

[54] V. Balzani, A. Credi, B. Ferrer, S. Silvi, and M. Venturi, Artificial molecular motors and machines: Design principles and prototypesystems, in *Molecular Machines*, edited by T. R. Kelly (Springer, Berlin, 2005), pp. 1–27.

[55] P. Reimann, Phys. Rep. **361**, 57 (2002).

[56] D. Chowdhury, Phys. Rep. **529**, 1 (2013).

[57] K. J. Challis, Phys. Rev. E **97**, 062158 (2018).